

Electronic Control System for Optimized Resonance Operation of Dielectric Elastomer Pumps through Self-Sensing

Matthias Baltes,* Benedikt Holz, Daniel Bruch, and Paul Motzki

In this work, a powerful electronic control system is developed for a dielectric elastomer (DE) pump, enabling it to achieve performance levels comparable to existing conventional pumps through resonance operation. The system incorporates a self-sensing approach to reconstruct the load pressure based on the pump's dynamic behavior. Using this approach, an optimal resonance operation is developed, where the resonance frequency adjusts according to the load pressure. This adaptive control strategy enables efficient operation by maintaining the pump in its resonance range, significantly improving energy efficiency and pumping performance. The presented solution highlights the potential of DE pumps to operate effectively without the need for external sensors, making them a promising alternative to conventional pumps for various applications.

use cases. Conventional pump technologies, including piston, diaphragm, and centrifugal pumps, are well-established and effective. However, they are subject to inherent limitations, particularly with regards to miniaturization, energy consumption, noise generation, and adaptability to novel, flexible system architectures. These constraints have led to growing interest in alternative actuation mechanisms, including those based on smart materials. Dielectric elastomers (DEs), as electroactive polymers, offer unique advantages for actuator applications due to their lightweight nature, high energy density, and inherent flexibility.^[8–11]

In recent years, DE-based actuation has emerged as a promising technology for innovative pump designs, potentially addressing some of the limitations of conventional systems.^[12–17]

This paper focuses on DE-based pumps and builds upon the results of a previous study.^[18] In that study, a DE pump was developed and successfully demonstrated, marking the first time such a system achieved performance levels suitable for real-world applications. A major challenge in earlier DE-based pump designs was their limited differential pressure, which often restricted their practical use. The newly developed pump addresses this limitation by achieving a vacuum with an absolute pressure of 300 mbar, corresponding to a differential pressure of 700 mbar, at a free flow rate of 0.6 L min^{−1}.^[18] This performance places the pump within a range comparable to conventional pump technologies and provides a solid foundation for further development and optimization.

Building on this foundation, the present study introduces two key advancements: integrated electronics and self-sensing capabilities. The goal of this work is to take the next step in advancing DE technology, specifically in the context of pump systems, toward a level where it can compete with conventional technologies and be considered a viable alternative for a wide range of applications. To achieve this, three main criteria must be met. The first criterion, demonstrating output power in the range of conventional pumps, has already been fulfilled in previous work. The remaining two aspects concern efficiency and cost. Here, the balance between performance metrics and the inherent advantages of DE technology, such as lightweight construction, flexible components, and the absence of rare earth materials, must be optimized. In terms of cost, significant progress has already been made on the mechanical side, thanks to low-cost base materials


1. Introduction

Pumps are critical components in a wide range of technical and industrial applications. As devices designed for the controlled transport of fluids, both liquids and gases, they are essential for enabling key processes in areas such as water supply,^[1,2] thermal management,^[1] chemical processing,^[3,4] medical technology,^[5,6] and transportation.^[7] Without pumps, many fundamental functions of modern infrastructure and technology would not be feasible.

The central role of pumps in these systems has driven continuous technological advancement, with a focus on improving efficiency, reducing size, and enhancing adaptability for specific

M. Baltes, P. Motzki
 Smart Material Systems
 Center for Mechatronics and Automation Technology (ZeMA gGmbH)
 Eschberger Weg 46, Saarbrücken 66121, Deutschland, Germany
 E-mail: matthias.baltes@imsl.uni-saarland.de

M. Baltes, B. Holz, D. Bruch, P. Motzki
 Department of Systems Engineering
 Department of Materials Science and Engineering
 Saarland University
 Eschberger Weg 46, Saarbrücken 66121, Deutschland, Germany

 The ORCID identification number(s) for the author(s) of this article can be found under <https://doi.org/10.1002/adem.202501204>.

© 2025 The Author(s). Advanced Engineering Materials published by Wiley-VCH GmbH. This is an open access article under the terms of the Creative Commons Attribution License, which permits use, distribution and reproduction in any medium, provided the original work is properly cited.

DOI: 10.1002/adem.202501204

and manufacturing processes that are compatible with automation. However, the most critical remaining challenge is the development of suitable driving electronics. Up to this point, the pump had to be operated using a Trek 5/80-HS high-voltage amplifier from Advanced Energy to reach 2300 V at 80 Hz.

The first part of this work focuses on designing a custom electronic driver that meets the performance requirements, operates from standard 24 V power supplies, and is compact and purpose-built for this application. The electronics are implemented and validated on the pump prototype to determine whether the desired output performance can be achieved with the generated voltage profile.

The second part of this work, explores the implementation of self-sensing functionality, which provides two key advantages: First, since the pump's resonance frequency is dependent on the applied load pressure, this relationship can be exploited to infer the actual pressure inside the system without requiring external pressure sensors. Second, by analyzing the system's frequency behavior, it becomes possible to determine its resonance state and adjust the drive frequency accordingly, ensuring optimal operation. This capability is then validated experimentally.

Based on these findings, in the third part of this work, a simplified control approach for optimal resonance operation is developed, ensuring that the pump consistently operates at its most efficient state while adapting to changing conditions.

In summary, this work advances DE-based pumps by transforming them into a fully integrated, sensor-less, and plug-and-play system. The result is a pump that can directly replace state-of-the-art conventional pumps while offering additional smart functionality, making DE technology a viable and competitive alternative in real-world applications.

2. Electronics

To fully exploit the potential of the developed DE pump, an appropriate driving electronics system is essential. The underlying electronics concept is based on a resonance-converter design originally developed for static dielectric elastomer (DE) applications.^[19,20] However, those applications were intended for systems with significantly lower capacitance. As a result, several adaptations, including the scaling of components such as a custom-made transformer, were necessary to make the design suitable for the requirements of the pump.

2.1. Electronics Concept and Design

For our high-voltage generation stage in the range of 2000 to 3000 V, we selected the Royer oscillator topology. This decision was based primarily on the availability of suitable transformers. In this voltage range, chamber-wound transformers are typically used, and such transformers were only available in configurations compatible with Royer circuits during our development.

An alternative approach considered during early stages of development was the flyback converter, which is widely used in high-voltage applications. However, we decided against this topology due to several limitations. Flyback converters typically generate high-pulsed currents, which result in increased EMI and stress on circuit components. Moreover, in order to reach

voltage levels in the 2–3 kV range, a flyback design would require additional voltage multiplier stages, such as cascaded diode-capacitor networks (e.g., Cockcroft–Walton multipliers). These additional stages not only increase the system's complexity, size, and cost but also negatively affect efficiency and voltage stability. Furthermore, the flyback topology requires external regulation circuitry, which contradicts our goal of developing a minimal, self-contained, and microcontroller-integrated solution.

In contrast, the Royer converter inherently regulates itself through feedback between the magnetic core and the oscillator circuit. This allows us to later implement a self-sensing control algorithm directly on a microcontroller. Instead of controlling switching behavior actively, the microcontroller can simply provide a reference signal, while the Royer circuit handles frequency and power regulation autonomously. This simplifies the system and enables adaptive operation without complex digital control logic.

We also briefly considered a third concept based on analog ESD (Electrostatic Discharge) generator topologies. These circuits produce high voltages by controlled discharge processes and typically provide a clear and clean output signal with low noise and distortion, which can be advantageous in precision applications. However, they generally require a separate high-voltage supply, involve more components, and are larger and more expensive compared to the Royer converter. Due to these drawbacks, and since the Royer topology already meets our requirements for stability and control without additional complexity, the analog ESD approach was deemed unnecessary for our application. In summary, the Royer concept offers the best balance between simplicity, efficiency, and adaptability for our specific application.

The centerpiece of this concept is a resonance transformer with a primary, a sensor/feedback, and a secondary winding. The transmission ratio between the primary and secondary winding is relatively large at 1:100 in order to generate the required high voltage of 2300 V. To ensure the voltage resistance, the secondary coil consists of a chamber winding in which the secondary winding is divided into a plurality of individual coils that do not exceed a maximum voltage potential of 500 V between two chambers. The sensor winding detects the energy content of the transformer core and thereby controls transistors, which, in combination with a capacitor connected to the primary winding, form a parallel resonant circuit. It is thus a self-oscillating parallel resonant circuit.

This generates an AC voltage of about 50 kHz on the primary side, which induces an AC voltage of an amplitude of 2300 V on the secondary side. This is rectified and fed to the DE system pump. In order to be able to generate an alternating signal at the pump, a discharging stage, consisting of cascaded MOSFETs was connected in parallel with the load, which can unload the stored charge of the DE in a controlled manner.

Via a voltage divider parallel to the load, the current voltage level of the DE system is measured and compared with a control signal. A corresponding control unit activates the resonant circuit via a high-side switch to bring charge to the DE system and thus cause the voltage to rise. In opposite, a signal to the discharge stage causes the voltage level at the DE system to fall. **Figure 1** shows the final PCB of the electronic concept.

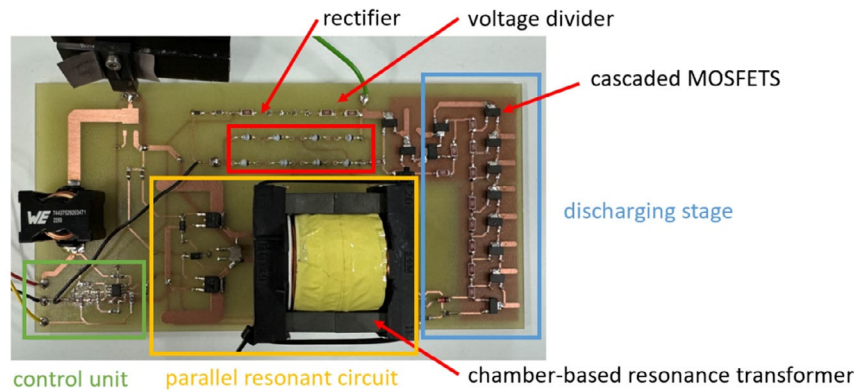


Figure 1. Assembled PCB of the electronic concept with individual components highlighted.

This concept was developed in other studies^[19,20] to control quasi-static systems and small loads. The following section outlines the requirements the pump places on the electronic concept and explains how the individual components must be adapted to meet these requirements.

2.2. Load Specifications and Electronics Dimensioning

The pump investigated in this work was designed in the context of a previous study.^[18] It consists of three main components: the pump chamber with integrated passive valves, four pre-stretched dielectric elastomer (DE) actuators, and a negative-rate bias spring (NBS) mounted underneath the actuators. The complete assembly is shown in **Figure 2**. Each DE actuator consists of a stack of 16 active dielectric layers and is pre-stretched by the negative-rate bias spring. The pre-stretching is essential to set the correct operating point of the actuators.^[21] In combination with the other mechanical components, particularly the bias spring and the load pressure, the pre-stretching enables the desired dynamic response of the system during operation.

The total capacitance of the four DE actuators connected in parallel varies between 55 and 66 nF, depending on the membrane displacement during the actuation cycle. This parameter is a key consideration for the design of the driving electronics and directly influences energy consumption and control requirements.

Another important factor for the electronics is the pump's intended operating frequency range. Figure 2 illustrates the dynamic response of the pump at different load pressures, specifically at atmospheric pressure (1000 mbar) and at its target minimum absolute pressure for vacuum generation (300 mbar). The pump is designed with a minimalistic approach and, as a result, achieves its optimal minimum pressure only when operated precisely at its resonance frequency. For a load pressure of 300 mbar, this resonance condition corresponds to a driving frequency of 80 Hz. Under continuous operation at 80 Hz, the pump reliably reaches its target pressure.

However, with a load of about 66 nF and a dynamic actuation of sinusoidal 80 Hz, the pump forms a significantly higher requirement. In the electronic system designed in this work, the chamber-based transformer had to be calculated and

increased in terms of energy to an ETD49 core. The resonance capacitor had to be chosen accordingly and optimized to the lowest possible ESR. Likewise, the final discharging-stage, which has to drive significantly more energy from the new load, had to be adjusted and expanded by a cooling concept for the MOSFETs cascade.

Previous studies have demonstrated that the pump exhibits a load-dependent change in stiffness (c_{system}), which leads to a shift in its resonance frequency (Equation (1)).^[18] To optimize pump performance across the entire operating range, it is necessary to ensure resonance operation at varying load pressures. At atmospheric pressure, the corresponding resonance frequency is 73 Hz. Consequently, the driving electronics must support an operational frequency range between 73 and 80 Hz to maintain optimal efficiency and performance under varying load conditions.

Two additional observations compared to previous studies are noteworthy. First, the pump prototype used in this work exhibits higher resonance frequencies. This increase is attributed to design modifications during assembly, where lightweight 3D-printed spacers were implemented on the moving axis instead of the heavier metal nuts previously used as distance holders. The reduction in moving mass (m_{free}) leads to an increased natural frequency of the system

$$f_r = \sqrt{\frac{c_{\text{system}}}{m_{\text{free}}}} \quad (1)$$

Second, a more pronounced damping effect is observed. Despite the higher resonance frequency at the maximum load condition (300 mbar), a smaller maximum amplitude would typically be expected. However, the measured amplitude is larger than anticipated. This behavior can be explained by a reduced damping in the system. Specifically, at maximum load pressure, the pump no longer performs mechanical work: no energy is extracted from the system, as the passive valves do not actuate. The actuators operate against a quasi-static air spring, and the pump no longer generates flow. Under these conditions, the absence of fluid movement results in minimal energy dissipation, effectively lowering the damping and leading to an increased amplitude in the dynamic response. Due to the reduced damping behavior, the pump reaches, at maximum differential pressure, a maximum amplitude in the frequency range

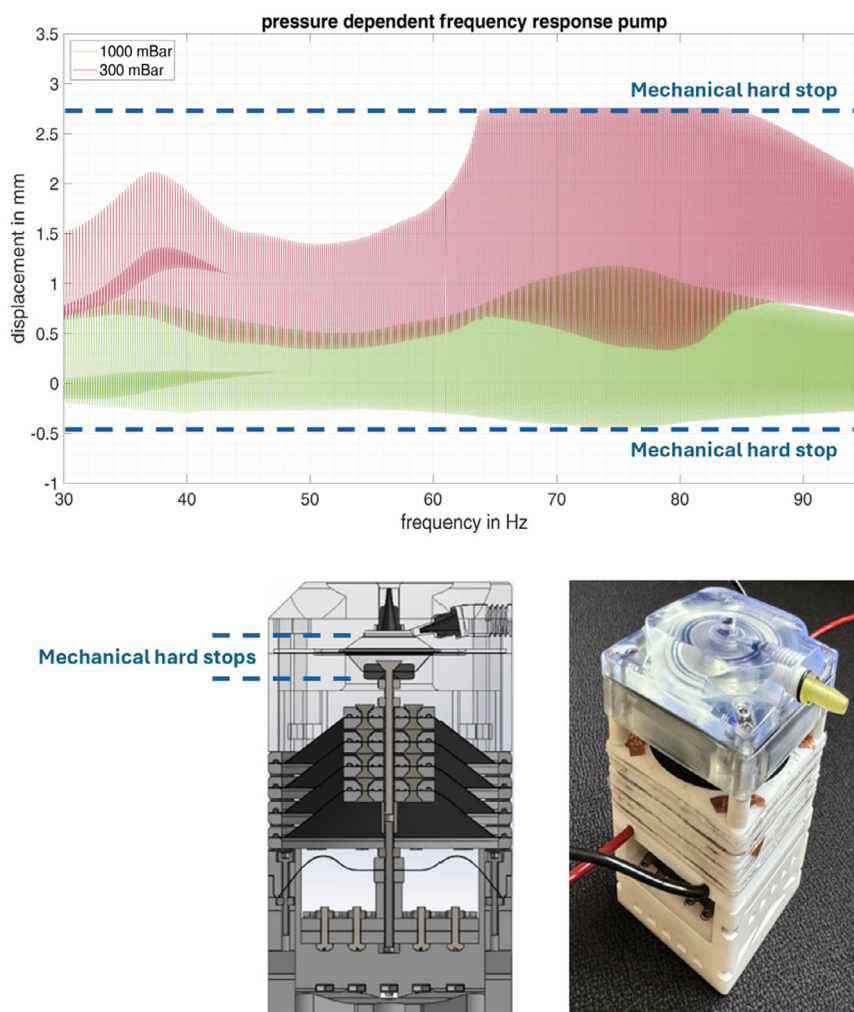


Figure 2. Pressure-dependent frequency behavior DE-based pump (left) and DE-pump (right).

from 65 to 80 Hz that exceeds the mechanical hard stop. As a result, the amplitude remains constant within this range. The hard stop thus distorts the otherwise well-defined peak amplitude for a certain frequency but has no significant effect on the pressure-dependent shift of the resonance frequency. This is demonstrated by the model and validation presented in source,^[18] where it is shown that the resonance frequency shift is not notably affected.

Based on these specifications, the electronics concept described in Section 2.1 is validated in the following section.

2.3. Electronics Validation with Pump Prototype

In order to validate the functionality and performance of the driving electronics in combination with the DE pump, a series of targeted measurements are conducted under varying operating conditions.

The pump is driven by the custom electronics at a constant frequency of 80 Hz, corresponding to its resonance frequency under maximum load pressure. As described in the previous

section, this is the required frequency to ensure the proper functionality of the pump. Measurements are carried out at ambient pressure, as well as at absolute pressures of 650 and 300 mbar. In each case, the voltage signal applied to the DE elements is recorded. Particular attention is given to verifying that the applied voltage maintains the target sinusoidal waveform with the required amplitude of 2300 V, and that the actual operating frequency matches the driving signal frequency. A supplementary video demonstrating the pump and its functional prototype is included with the supplementary materials.

Additionally, it is ensured that the DE actuators are fully discharged during each cycle. The discharge current is monitored and analyzed, as this data will be important for further investigations in the field of self-sensing. The voltage signals, along with their corresponding load pressures, are shown in **Figure 3**.

Several effects can be observed in the measurements. Firstly, in all cases, the electronics does not reach 0 V but instead exhibit a small offset of 100 V. This offset is negligible in terms of functionality, since the actuation force of the DEs depends quadratically on the applied voltage. As a result, the contribution from the

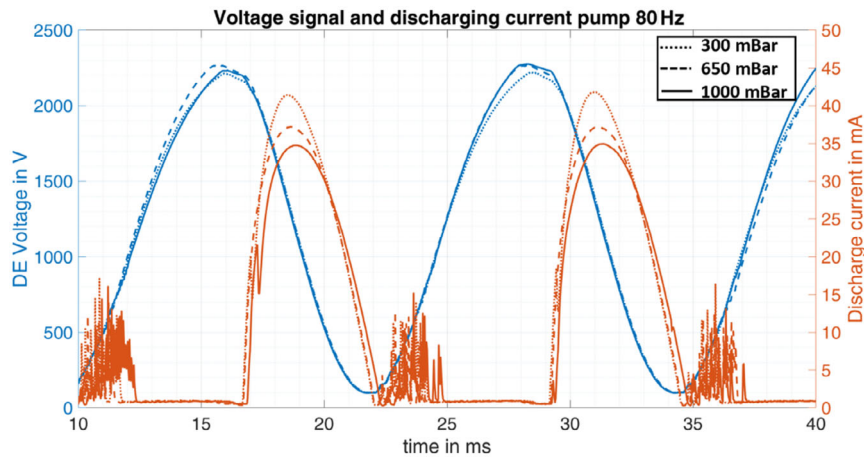


Figure 3. Resulting high-voltage signal and discharge current pump actuator for different load pressures.

lower voltage range is almost insignificant. Additionally, it is noticeable that the maximum amplitude achieved is load-dependent, with different amplitudes observed at different load pressures. This is due to the variable capacitive load. In resonance, as shown in Figure 2, the DE actuator is further deflected, causing an increase in capacitance. As a result, electronics must supply more charge to the DE elements in order to generate the same voltage. Although the maximum amplitude might be slightly smaller under varying load conditions, it is still sufficient to generate the required voltage. This can be verified with a pressure sensor (Honeywell HSCDANN001BA2A3), which shows a value of minimal 300 mbar absolute pressure, confirming that the voltage is adequate to achieve the desired performance. Furthermore, the measurements demonstrate that the frequency follows the desired waveform precisely enough, with the form closely resembling a sine wave. Small deviations occur at maximum voltage and simultaneous maximum load (maximum deflection of the DEs at 300 mbar load pressure). In this case, the electronics is unable to charge the high capacitance quickly enough. The controller is currently configured to deliver maximum energy in this specific range. However, these settings have an additional consequence: at the beginning of the charging phase, a charging current can be observed that appears as noise. In this phase, the DE (Dielectric Elastomer) is still not fully actuated, meaning it has a lower capacitance. Additionally, the sinusoidal reference signal is relatively flat, so the DE requires less energy during charging. Since the controller is tuned to operate optimally around 2300 V, it tends to overshoot in the lower region of the sine wave. As a result, the discharge stage is activated to counteract the overshoot and adjust the voltage to match the reference. In the future, the controller can be further optimized, as the system is not yet operating at maximum efficiency.

The described effect, in which the DE actuator is further deflected in resonance, leads to an increase in capacitance. This higher capacitance allows more charge to be stored on the DE elements for the same applied electrical voltage. This phenomenon can also be utilized for the self-sensing effect, as the increase in capacitance is directly related to the actuator's displacement, enabling the system to sense its own behavior.

The approach for implementing this self-sensing method will be described in detail in the next section.

3. Self-Sensing

Self-sensing in dielectric elastomer actuators is commonly associated with correlating the actuator's deformation with its capacitance. This allows for determining the actuator's position by reconstructing it through capacitance measurements. However, such an approach is not necessary for the pump, as pressure can be inferred with less complex information. This study demonstrates that the load pressure of the pump can be reconstructed without requiring the high-frequency superimposition typically used in other self-sensing systems.^[22–24] Instead, simpler measurements provide sufficient data to make accurate pressure estimations.

3.1. Self-Sensing Concept for Pressure Reconstruction

In Section 2, it was already described that the electronics must apply different amounts of charge to the DE depending on the load pressure. This is due to the load pressure-dependent shift of the resonance, resulting in a different maximum amplitude at a constant resonance frequency. The mechanical maximum amplitude also directly influences the capacitance of the DE. During the discharge of the DE, the charge previously applied must be removed, and this occurs through the discharge stage of the electronics.

This effect is utilized in the case of our pump to reconstruct the pressure. The charge ΔQ flowing out of the DE during discharge can be determined by measuring the voltage $U_{\text{discharge}}$ across the resistors of the discharge stage $R_{\text{discharge}}$

$$I = \frac{U_{\text{discharge}}}{R_{\text{discharge}}} \quad (2)$$

Since this resistance is constant, the current I can be calculated directly. By integrating this current over a discharge cycle

(t_{start} until t_{end}), the total charge that flows out of the DE during this cycle can be measured

$$\Delta Q = \int_{t_{\text{start}}}^{t_{\text{end}}} I dt \quad (3)$$

Using the charge ΔQ and the known maximum voltage U applied to the DE at the beginning of the discharge phase, the capacitance C can be calculated

$$C = \frac{\Delta Q}{U} \quad (4)$$

The schematic approach for the capacity reconstruction is illustrated in **Figure 4**.

This capacitance depends on the geometry of the DE, including its area A and thickness d , which in turn depend on its maximum amplitude during actuation, the electric field constant ϵ_0 , and the material constant ϵ_r , in our case for silicone

$$C = \epsilon_0 \epsilon_r \frac{A}{d} \quad (5)$$

In the case of our DE, it is a COP-DE (circular out-of-plane) actuator. Its geometric structure resembles a truncated cone, where the lateral surface area A can be calculated from the maximum deflection s_{max} as well as the outer radius R and inner radius r .

$$A = \pi(R+r)\sqrt{(R-r)^2 + s_{\text{max}}^2} \quad (6)$$

The incompressibility of the dielectric elastomer (DE) implies that, given the initial film thickness d_0 (unstretched: $50 \mu\text{m}$) and the initial area A_0 , the current thickness d can be calculated using volume conservation

$$d = \frac{A_0 d_0}{A} = \frac{\pi(R^2 - r^2)d_0}{\pi(R+r)\sqrt{(R-r)^2 + s_{\text{max}}^2}} \quad (7)$$

Using Equations (2)–(7), it is therefore possible to reconstruct the maximum amplitude from the measured discharge voltage.

To validate this concept, measurements are conducted in the following section at two different driving frequencies, 70 and 80 Hz. During these tests, the discharge currents are measured at three different load pressures. Based on the recorded discharge currents, the maximum capacitance of the system can be calculated. This allows for a direct correlation between the capacitance and the pressure-dependent behavior of the pump, specifically its resonance frequency and amplitude characteristics.

3.2. Self-Sensing Validation with Pump Prototype

In this section, the frequency response of the pump is first recorded for three different load pressures. To do this, the pump is driven with a sinusoidal signal of increasing frequency, starting at 30 Hz and ramping up to 95 Hz. A laser displacement sensor (Keyence LK-G87) is used to measure the frequency-dependent amplitude of the pump membrane during operation. This measurement is performed for the three selected absolute pressures of 1000, 300, and 650 mbar.

To ensure that the pressure remains constant throughout the measurement, a buffer volume is connected to the pump's inlet valve. This setup minimizes pressure fluctuations during the frequency sweep, ensuring stable conditions for accurate data collection. The pressure is monitored, as before, using a pressure sensor. For venting the system, an exhaust valve is installed. At the discharge electrode itself, the high-voltage signal can be measured, while on the ground side, the discharge current is recorded. The complete setup is shown in **Figure 5**.

In a second series of measurements, the discharge currents are recorded for the same load pressures in the buffer tank. During these tests, the pump is driven at two constant exemplary actuation frequencies, 70 and 80 Hz. Two example frequencies are sufficient, as the frequency range in which the pump operates is inherently very narrow due to its mechanical design. Moreover, as will be shown later, there is no observable dependence of the capacity on the operating frequency within this range. Following the schematic procedure in **Figure 4**, the total charge flowing from the DE during discharge can be calculated by integrating the discharge current over a complete discharge cycle. **Figure 6** presents the results of both measurement series, with the data for 70 Hz a) and for 80 Hz b). The total charge obtained from these measurements is then used to calculate the maximum capacitance of the DEs in the pump actuator at the beginning of the discharge cycle.

To validate the relationship between the maximum amplitude and the capacitance at the beginning of the discharge cycle, the capacitances reconstructed from the measurements are compared with the actual capacitance of the discharge electrodes (DEs). For this purpose, the DEA itself is characterized. Using a linear actuator, the DEA is moved from its initial, undeflected position to its maximum deflection corresponding to the application scenario. Specifically, the hard stop of the pump chamber, which results in a 15 mm deflection of the DE. During this process, the capacitance is measured with an LCR meter. **Figure 7** shows the capacitance as a function of displacement. In this plot, the reconstructed capacitance values obtained during dynamic operation are also plotted according to their respective deflections

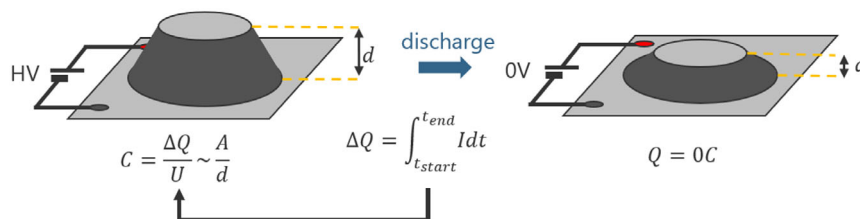


Figure 4. Schematic approach for maximum capacity reconstruction at the beginning of the discharge phase.

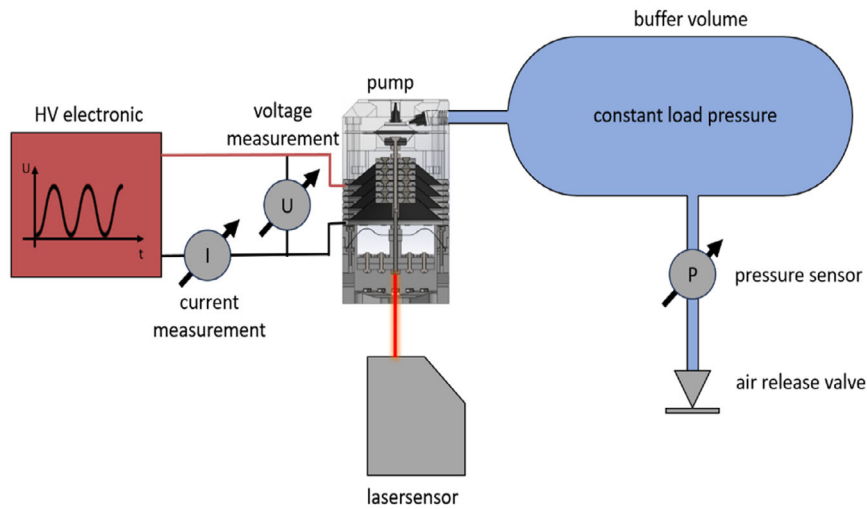


Figure 5. Overview measurement setup for self-sensing validation.

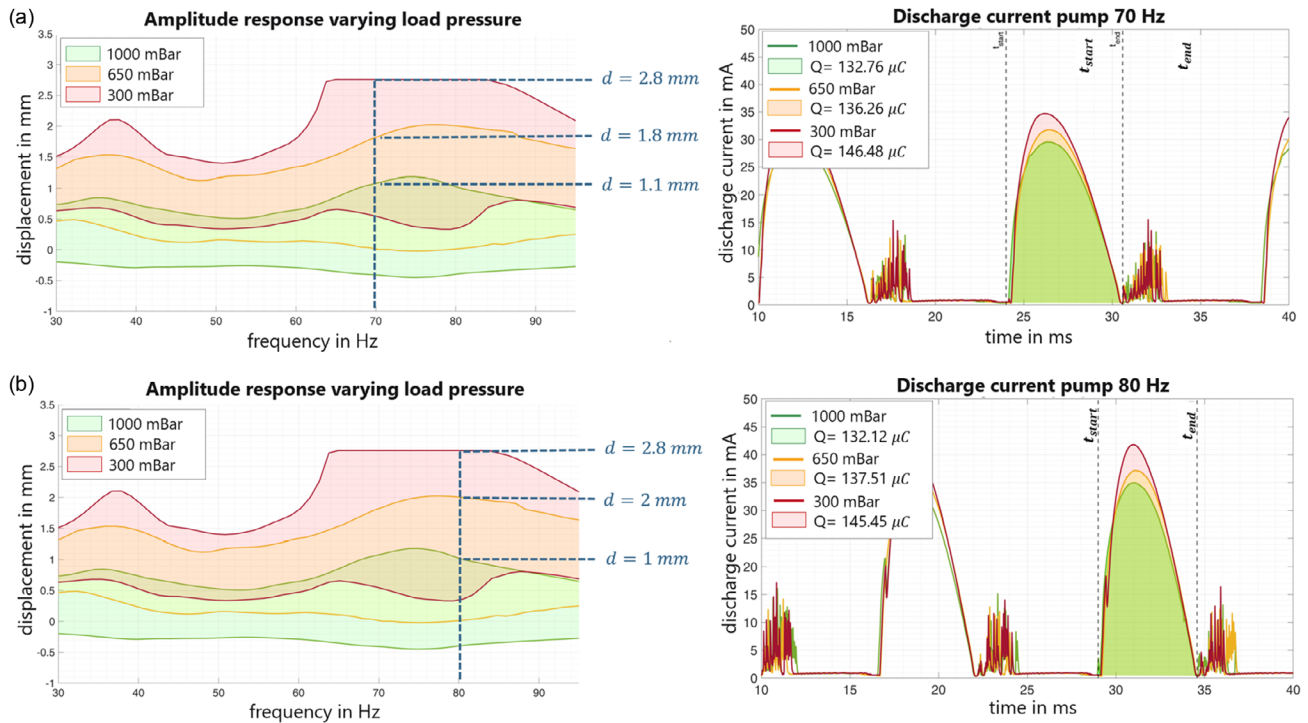


Figure 6. Load pressure-dependent frequency behavior and charge calculation DE-based pump: a) 70 and b) 80 Hz.

(Figure 6). For better clarity, the mechanical hard stops and the static equilibrium position of the pump actuator (corresponding to a deflection of 0 mm in the pump) are also indicated.

An offset can be observed between the dynamically reconstructed capacitance values and the directly measured ones. This discrepancy can be explained by the voltage curves shown in Figure 3. The voltage curve exhibits an offset of 100 V, which means that the dielectric elastomer (DE) is not fully discharged as assumed in the schematic approach illustrated in Figure 4. Instead, it retains a residual charge. This remaining charge

corresponds to the product of its capacitance at minimal displacement and the residual voltage of 100 V still applied to the DE.

By analyzing the frequency response (Figure 6), the corresponding minimal amplitude can be determined for each combination of actuation frequency and applied pressure. Using the capacitance-displacement graph (Figure 7), the minimal capacitance C_{\min} associated with this state can be identified. Based on these two values (the minimal capacitance and the residual voltage), the remaining charge can be calculated and subsequently taken into account in the reconstruction process. By applying

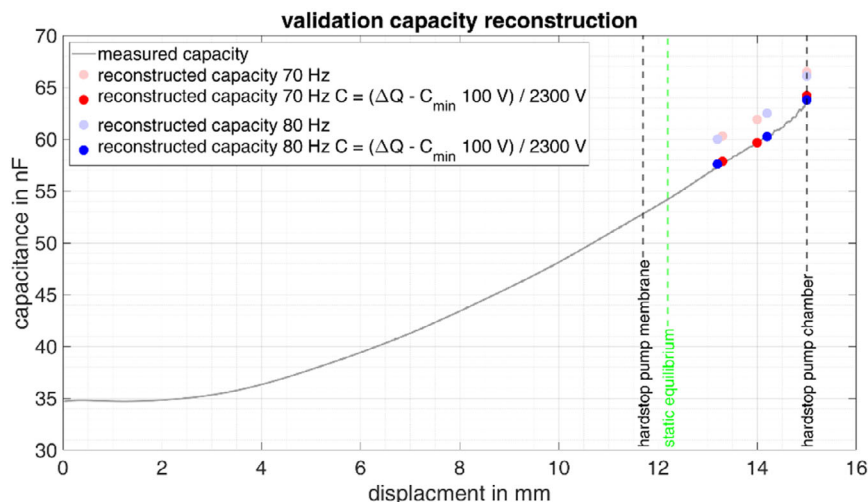


Figure 7. Comparison capacity reconstruction and measured capacitance DEA.

the correction factors, a very good agreement between the reconstructed and measured capacitance values is achieved. However, a limitation of this approach is that it cannot be applied in real-time operation. The objective is to measure the applied pressure. For a known actuation frequency, each pressure level can be assigned a corresponding maximum amplitude. This relationship can be derived either from the frequency response and a dedicated measurement series or by using the model and simulation developed in previous work to describe the dynamic behavior. In order to calculate the correction factor shown in Figure 7, both the actuation frequency and the applied pressure must be known. While the actuation frequency is given, the applied pressure is not directly available in an online application. To enable capacitance reconstruction with sufficient accuracy despite this limitation, a constant correction factor is used. This factor is determined based on a residual voltage of 100 V and the minimal amplitude at static equilibrium. The minimal amplitudes for different pressures and frequencies are concentrated within a range of approximately ± 0.5 mm around the static equilibrium position. Accordingly, the corresponding minimal capacitances vary within ± 1 nF. Since the residual voltage of 100 V is relatively small compared to the maximum voltage of 2300 V, the variation in residual charge resulting from capacitance fluctuations of ± 1 nF is negligible in relation to the total charge corresponding to 60–66 nF at 2300 V.

Figure 8 compares the capacitance reconstruction using the previously applied correction factor 1) and the constant correction factor derived from the capacitance at static equilibrium b). As expected, the deviation from the actual capacitance value is larger for this simplified approach compared to the more complex, physically accurate method. However, it can be observed that even in cases of maximum deviation in the measurements, the capacitance differs by only 0.5 nF from the actual value. Given the nearly linear relationship between capacitance and displacement within the pump's operating range (11.7–15 mm), this corresponds to an error of ≈ 0.1 mm over a total working range of 3.3 mm, which corresponds to an error of about 3%.

This section demonstrates that the maximum amplitude can be reconstructed using the discharge current. By utilizing the dynamic behavior, which was modeled, simulated, and validated in previous work, the applied pressure can then be reconstructed for a known actuation frequency. This approach reaches its limit when the pump attains the same maximum amplitude at different load pressures. This situation can occur if the pump is not optimally designed for the specific application. If the pump is oversized, it will reach the hard stop even at relatively low maximum differential pressures, thereby limiting the accuracy of pressure reconstruction. However, since the primary goal is to maintain pump efficiency as high as possible, this effect should generally not occur under normal operating conditions.

To summarize, the pressure can be determined without the need for an external sensor, within the accuracy limits of the model and its agreement with the dynamic behavior. Although this approach does not match the precision of a dedicated pressure sensor, it provides a feasible solution within a range where many pump-related parameters can be assessed. For example, simple status measurements, such as verifying whether the target pressure has been reached, can be performed. To do this, it is only necessary to know the maximum amplitude at the given actuation frequency for the desired pressure, either through the model or measurement. Optimized control, which will be investigated in the next section, can also be implemented based on this. The resonance frequency and maximum amplitude for different applied pressures are known, and with the appropriate control, the pump can operate optimal within its resonance range, from 73 Hz at ambient pressure to 80 Hz at 300 mbar absolute pressure.

4. Simple Control Strategy for Resonance Operation

In the final step, a simplified adaptive control strategy for the pump is implemented, based on the insights obtained in the previous sections. “Adaptive” in this context means that the control

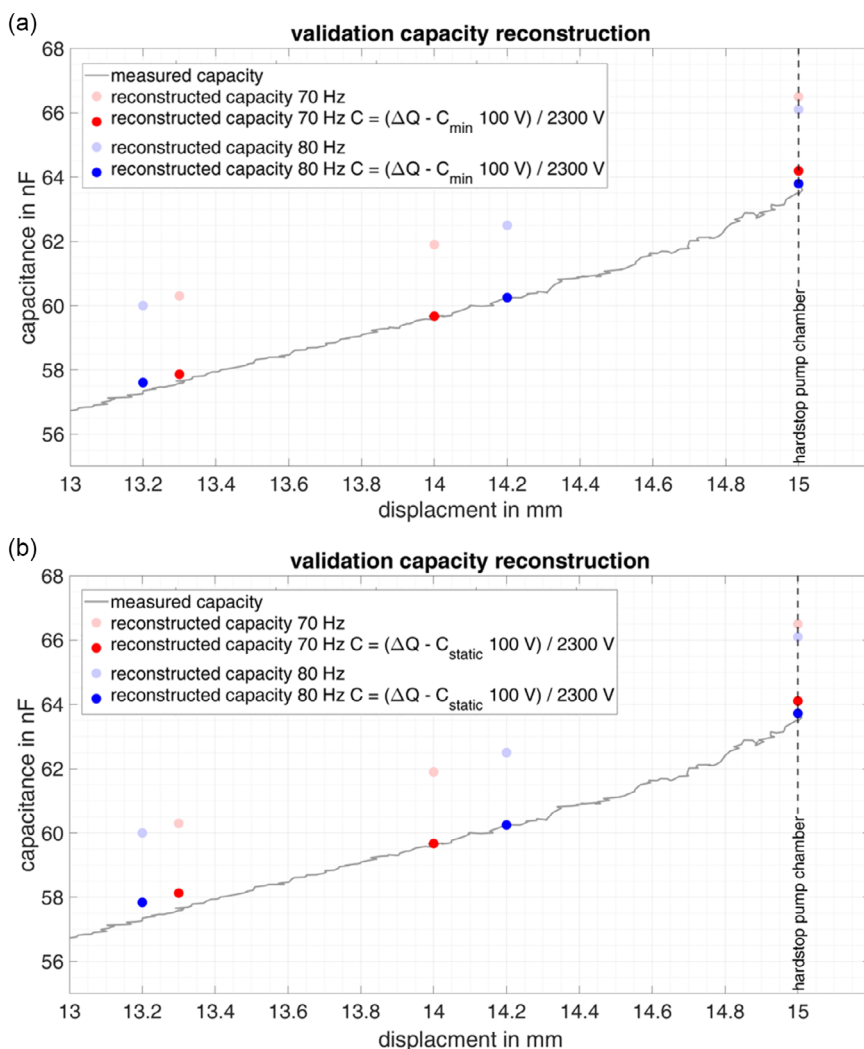


Figure 8. Comparison of a) complex capacity reconstruction and b) simplified approach.

frequency initially starts at 73 Hz, which corresponds to the resonance frequency under the given ambient pressure. The pump begins operating at this frequency to generate vacuum. Using the method described in the preceding chapter, the maximum amplitude can then be calculated. Based on the load-dependent amplitude profile and the appropriate model for the pump, the pressure can be reconstructed. As the applied pressure changes, the resonance frequency shifts. Therefore, the control frequency is iteratively adjusted to ensure that the operating frequency remains aligned with the current resonance frequency. **Figure 9** illustrates the setup of this simplified control methodology.

In the simplest case, this can be implemented on a microcontroller using look-up tables and threshold values. Fixed values in the look-up table are used to check whether the pressure has fallen below a defined threshold. If this is the case, the working frequency is gradually increased. This process continues for each new working frequency until the minimum absolute pressure is reached. At this point, the working frequency is 80 Hz, which corresponds to the resonance frequency for 300 mbar.

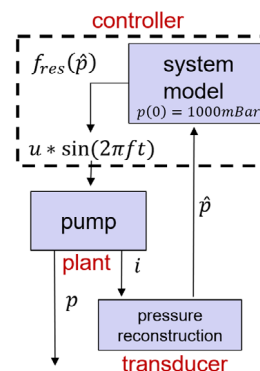


Figure 9. "Adaptive" control methodology DE-based pump.

To compare the efficiency, two experiments are conducted. As a reference, in the first experiment, the pump is operated at a constant frequency of 80 Hz. This frequency is required

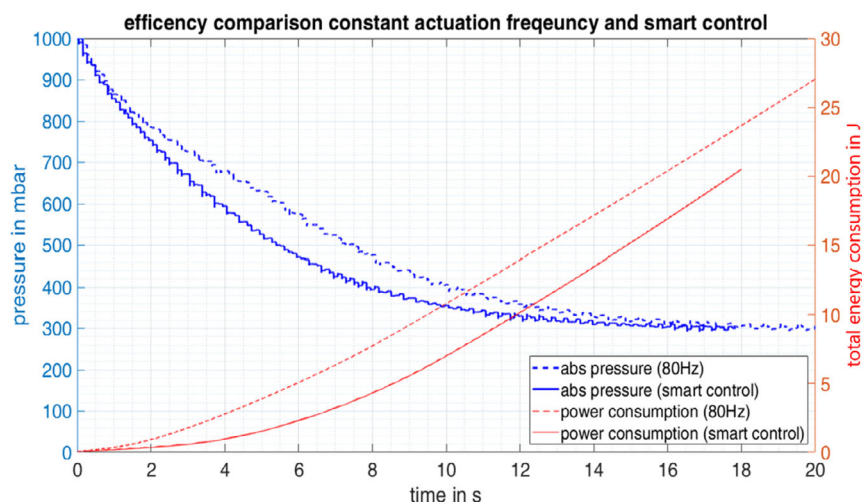


Figure 10. Efficiency comparison 80 Hz actuation and adaptive controlled actuation.

to reach the minimum absolute pressure. The pump builds the vacuum in a closed tank. During this process, the electrical power supplied to the pump and the pressure inside the tank are measured. The measurement continues until a pressure of 300 mbar is reached.

Afterward, the same tank setup is used, but the pump is controlled with the smart control strategy, starting at 73 Hz and increasing up to a maximum of 80 Hz as the minimum absolute pressure is approached. The results are shown in **Figure 10**.

Two effects can be observed. Firstly, the pump requires 2 s less to achieve the same vacuum level (18 instead of 20 s). This is because, despite operating at a lower frequency, the pump achieves a higher flow rate. The flow per cycle is significantly greater, resulting in an overall flow rate (frequency multiplied by flow per cycle) that is higher than at the constant higher frequency. This is due to the fact that, in resonance operation, the pump achieves a larger stroke, allowing it to compress and decompress more volume per cycle, and thus deliver a higher flow rate. The second effect concerns the energy consumption required to generate the vacuum. Until the minimum absolute pressure is reached, the pump operating at a constant 80 Hz consumes 27 J, whereas in smart resonance mode, it consumes only 20 J. The energy considered here corresponds to the difference between the energy required to charge the actuators and the theoretically recoverable energy during discharge. At present, this does not reflect the actual consumption of the pump, since the energy during discharge is not yet recovered. However, this aspect presents an opportunity for further optimization in the future, which will be discussed in the conclusion.

5. Conclusion

DE-based pumps have been extensively studied in previous works. In this study, the focus is not on the development of the pump itself, but on the electronics, control system, self-sensing capabilities, and optimization strategies for the existing pump.^[18] The DEA, which was developed earlier, already outperforms

current technology in the field of DEAs in terms of performance and offers output levels comparable to industrial pumps. However, it is currently driven by expensive laboratory electronics. This work addresses this challenge by developing compact and cost-effective electronics that can control the pump with the desired performance.

Another key aspect of this study is the investigation of the advantages of DE-based pumps in comparison to conventional pumps. A frequently cited feature of DEAs is their self-sensing capability. It is demonstrated that the load pressure of the pump can be reconstructed by measuring the discharge current on the ground side of the DEA. Since the entire system's behavior is considered, including the influence of various components and load pressures on the dynamic behavior, it is not necessary to continuously measure capacitance during operation, as is commonly assumed in self-sensing systems. Instead, it is sufficient to identify which simple measurements can be used to infer the desired output parameters.

One example of how the pump operates smartly and differentiates itself from the state-of-the-art is the optimal resonance operation without the need for external sensors. The self-sensing capability allows the pump to autonomously adjust its working frequency to the load pressure dependent resonance frequency, resulting in an energy saving of $\approx 25\%$.

An important future direction is the continued optimization of the pump's efficiency. One interesting approach could be the operation of two pump chambers in series, which is common in many applications to achieve higher differential pressures with the given pump chamber design. These chambers often reach their limit due to dead volume, for example, inside the valves. In such setups, pump chambers are typically operated with a 180° phase shift. This concept, common in conventional pumps, inherently offers interesting possibilities for energy recovery. For example, by exploiting the 180° phase shift in the drive signals, half of the charge could be transferred from one actuator of a chamber to the other through targeted switching.

For applications where a single pump chamber is sufficient, pure energy recovery concepts can also be pursued. However,

there is always a trade-off between efficiency improvement and the additional complexity and cost of implementing such electronics. In contrast, the concept involving two chambers operated in series complements this well, as it enables energy recovery with relatively low added effort.

Acknowledgements

Open Access funding enabled and organized by Projekt DEAL.

Conflict of Interest

The authors declare no conflict of interest.

Author Contributions

Matthias Baltes: conceptualization (lead); data curation (lead); software (lead); writing—original draft (lead). **Benedikt Holz:** writing—original draft (supporting). **Daniel Bruch:** writing—review & editing (equal). **Paul Motzki:** conceptualization (supporting); writing—review & editing (equal).

Data Availability Statement

Research data are not shared.

Keywords

dielectric elastomers actuators, electro-active polymers, resonance operations, self-sensing, vacuum pumps

Received: May 3, 2025

Revised: June 12, 2025

Published online: July 1, 2025

- [1] S. Yedidiah, *Centrifugal Pump User's Guidebook*, Springer Science & Business Media, Springer **1996**.
- [2] M. Z. Youssef, *IEEE Trans. Ind. Electron.* **2015**, 62, 3277.
- [3] E. Leati, R. Scheidl, A. Ploekinger, *On the Dynamic Behavior of Check Valves for High Frequency Oscillation Pumps*. *ASME/BATH Symp. on Fluid Power and Motion Control* **2013**.

- [4] J. Klespitz, L. Kovács, in *2014 IEEE 12th Inter. Symposium on Applied Machine Intelligence and Informatics (SAMII)* **2014**, pp. 191–194.
- [5] K. M. Pos, *Biochim. Biophys. Acta (BBA) - Proteins Proteomics* **2009**, 1794, 782.
- [6] L. Cao, S. Mantell, D. Polla, *Sens. Actuators A Phys.* **2001**, 94, 117.
- [7] U. Kemmner, M. Rollwage, K. Rose, *SAE International Congress and Exposition*, Feb. **1987**.
- [8] *Dielectric Elastomers as Electromechanical Transducers*, Elsevier **2008**.
- [9] Z. Xing, J. Zhang, D. McCoul, Y. Cui, L. Sun, J. Zhao, *Soft Rob.* **2020**, 7, 512.
- [10] R. Kornbluh, R. Pelrine, *Dielectric Elastomers as Electromechanical Transducers* (Eds: F. Carpi, D. De Rossi, R. Kornbluh, R. Pelrine, P. Sommer-Larsen), Elsevier, Amsterdam **2008**, pp. 33–42.
- [11] S. Michel, X. Zhang, M. Wissler, C. Löwe, G. Kovacs, *Polym. Int.* **2009**, 59, 391.
- [12] M. Smith, V. Cacucciolo, H. Shea, *Science* **2023**, 379, 1327.
- [13] S. Ho, B. Hritwick, Y. Yoke, G. Hareesh, M. Winn, Z. Jian, H. Choon, *J. Intell. Mater. Syst. Struct.* **2017**, 28, 3054.
- [14] Y. Wang, Z. Li, L. Qin, G. Caddy, C. H. Yap, J. Zhu, *J. Appl. Mech.* **2018**, 85, 101003.
- [15] G. Mao, L. Wu, Y. Fu, Z. Chen, S. Natani, Z. Gou, X. Ruan, S. Qu, *IEEE/ASME Trans. Mechatron.* **2018**, 23, 2132.
- [16] A. Kumar, D. Ahmad, K. Patra, *Electromechanical Characterization of Dielectric Elastomer Actuator based Pump for Optimum Volume Flow Rate*. *National Conf. on Advanced Materials, Manufacturing and Metrology* **2018**.
- [17] J. Chavanne, J. Haenni, T. Martinez, D. Moser, A. Walter, M. Almanza, F. Clavica, Y. Civet, Y. Perriard, in *2020 23rd Inter. Conf. on Electrical Machines and Systems (ICEMS)*, IEEE, Nov. **2020**, pp. 380–383.
- [18] M. Baltes, D. Bruch, P. Motzki, *Eng. Rep.* **2025**, 7, e70237.
- [19] S. Lenz, B. Holz, S. Hau, S. Seelecke, in *ACTUATOR 2018; 16th Inter. Conf. on New Actuators* **2018**, pp. 1–4.
- [20] C. Perri, S. Lenz, G. Rizzello, S. Seelecke, D. Naso, in *2021 IEEE 30th Inter. Symposium on Industrial Electronics (ISIE)*, IEEE, Jun. **2021**, 01–06.
- [21] M. Hodgins, S. Seelecke, *Proc. of SPIE - The Inter. Society for Optical Engineering*, vol. 7644, Mar. **2010**.
- [22] G. Rizzello, P. Serafino, D. Naso, S. Seelecke, *IEEE Trans. Rob.* **2020**, 36, 174.
- [23] J. Prechtel, M. Baltes, K. Flaßkamp, G. Rizzello, *IEEE/ASME Trans. Mechatron.* **2024**, 29, 4365.
- [24] S. Gratz-Kelly, T. F. Krüger, S. Seelecke, G. Rizzello, G. Moretti, *Sens. Actuators A Phys.* **2024**, 372, 115332.